A Compact Wave Source Condition for the Pseudospectral Time-Domain Method

Tae-Woo Lee, *Student Member, IEEE,* and Susan C. Hagness, *Senior Member, IEEE*

***Abstract*—An incident wave source condition that specifies the field at a single grid point is problematic for the pseudospectral time-domain (PSTD) method because of the spatial Fourier transforms inherent in the algorithm. Previously, it had been suggested in the literature that a spatially smoothed source spanning several grid cells in each direction was required to avoid aliasing errors referred to as Gibbs phenomena. Here, we show that a spatially compact wave source condition spanning only two spatial grid cells in each directions eliminates the numerical artifacts induced by this aliasing/Gibbs effect. We demonstrate the successful implementation of this source condition in two practical PSTD modeling examples: fundamental mode excitation in a dielectric slab waveguide and cylindrical wave excitation via an infinite electric line source in a two-dimensional grid.**

***Index Terms*—Finite-difference time-domain (FDTD) methods, Maxwell equations, pseudospectral time-domain (PSTD) method, source conditions.**

I. Introduction

THE pseudospectral time-domain (PSTD) method of solving the time-dependent Maxwell's curl equations [1] uses the differentiation theorem for Fourier transforms to numerically implement the spatial derivatives in Maxwell's equations on an unstaggered, collocated space lattice. According to the Nyquist sampling theorem, this spatial-differencing process converges with "infinite order" accuracy for grid-sampling densities of two or more points per wavelength. Thus, the PSTD method is a promising scheme for reducing numerical dispersion artifacts. Accordingly, it has been shown to be more computationally efficient than the standard finite-difference time-domain (FDTD) algorithm [2] for several classes of engineering problems [3]–[5].

In PSTD, the implementation of a spatially compact incident wave source condition requires special care for the following reason. A source which specifies the field at a single grid point with a temporal driving function represents a spatial delta function. This type of point source causes difficulties for the fast Fourier transforms (FFTs) inherent in the PSTD algorithm and introduces aliasing errors which have been referred to as Gibbs phenomena in previous publications.

To date, the issue of PSTD source implementation has been discussed only briefly in the literature. Li and Chen proposed a local-in-time, global-in-space initial-condition excitation on both the electric and magnetic field components [6]. This approach inherently avoids the problem of Gibbs phenomena as long as the spatial distribution of the fields is smooth. However, since the electric and magnetic fields are staggered in time, this technique requires the desired spatial waveform to be analytically time-marched by one-half of a time step. The exact time evolution is not known for many engineering problems of interest and must be approximated, thereby introducing a different type of source-related error. A spatially compact wave source specified with a temporal driving function is typically preferred in most practical modeling problems. Liu proposed the use of a global-in-time, local-in-space source condition comprised of a spatially smoothed source "occupying a volume of only a few (4–6) cells" in each grid direction [3]. However, no specific guidelines or details were provided.

In this letter, we discuss the implementation of two classes of spatially compact wave sources for coupling energy into the PSTD lattice: 1) transparent current sources, and 2) hard field sources. We show that a compact source spanning only two spatial grid cells in each direction completely cancels the errors due to Gibbs phenomena. In Section II, we propose and demonstrate the performance of the two classes of source conditions in the context of a one-dimensional (1-D) linear problem. In Section III, we illustrate the successful implementation of these source conditions in the context of two practical two-dimensional (2-D) modeling examples: fundamental mode excitation in a dielectric slab waveguide and cylindrical wave excitation via an infinite electric line source in a 2-D grid.

II. Transparent Current and Hard Field Sources

Consider a spatially localized electric current source located at $i = i_s$ in a 1-D grid designed for TEM wave propagation along the x-axis with the electric field vector oriented in the z direction. This current source can be implemented in the electric-field update equation as follows:

$$E_z|_{i_s}^{n+1} = E_z|_{i_s}^{n} + \frac{\Delta t}{\epsilon_{i_s}} \left.\frac{\partial H_y}{\partial x}\right|_{i_s}^{n+\frac{1}{2}} + f(t)|^{n+\frac{1}{2}} \qquad (1)$$

where $f(t)$ is the temporal driving function that represents a linearly scaled version of the electric current density term in Maxwell's equations. (For simplicity, we have assumed a lossless medium.) We define a single current source as the case where (1) is implemented at only one grid point, and a twin current source as the case where two identical current sources are located at adjacent grid points.

Before we investigate the performance of these source conditions, we analytically relate the amplitude and phase of the

Manuscript received April 17, 2004; revised July 8, 2004. This work was supported by the National Science Foundation Presidential Early Career Award for Scientists and Engineers (PECASE) ECS-9985004.

The authors are with the Department of Electrical and Computer Engineering, University of Wisconsin, Madison, WI 53706 USA (e-mail: hagness@engr.wisc.edu).

Digital Object Identifier 10.1109/LAWP.2004.835754

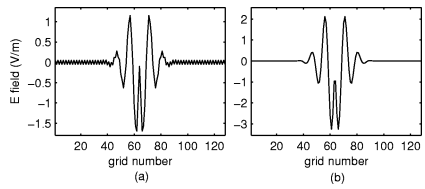

Fig. 1. Spatial distribution of the electric field in a 1-D PSTD grid at an early-time snapshot. A ramped sinusoidal wave is excited in the center of the grid. (a) Single current source is located at $i_s = 64$. (b) Two identical current sources are located at $i_{s1} = 63$ and $i_{s2} = 64$.

electric field component of a radiated sinusoidal wave to the amplitude and phase of the twin-source temporal driving function. To derive this relation, we establish a reference point $(x = 0)$ between the two adjacent point sources, $f_1(t) = A_o \sin(\omega t + \phi)$ located at $x = -\Delta x/2$ and $f_2(t) = A_o \sin(\omega t + \phi)$ located at $x = +\Delta x/2$. The electric field observed at $x_{\rm obs} > 0$, due to $f_1(t)$, can be written as follows:

$$E_{z_1}(x_{\rm obs}, t) = E_o \sin\left[\omega t - k_x\left(x_{\rm obs} + \frac{\Delta x}{2}\right) + \phi\right] \quad (2)$$

where $E_o = -A_o \Delta x \sqrt{\varepsilon_r}/(2c\Delta t)$. Likewise, the electric field due to $f_2(t)$, observed at $x_{\rm obs} > 0$, can be written as

$$E_{z_2}(x_{\rm obs}, t) = E_o \sin\left[\omega t - k_x\left(x_{\rm obs} - \frac{\Delta x}{2}\right) + \phi\right]. \quad (3)$$

The linear superposition of the two waves generated by the individual sources yields the total observed field

$$E_z(x_{\rm obs}, t) = 2E_o \cos\left(\frac{k_x \Delta x}{2}\right) \sin(\omega t - k_x x_{\rm obs} + \phi). \quad (4)$$

Equation (4) clearly shows that the electric field component of the TEM wave launched by the pair of identical current sources has a well-defined phase and amplitude related directly to the temporal driving function.

Next, we evaluate the performance of the single- and twin-source schemes in 1-D PSTD simulations. In the first simulation, we implement a single current source in the center of the grid at $i_s = 64$ using a ramped sinusoid as the temporal driving function. In the second simulation, we implement a twin current source, that is, two adjacent current sources at $i_{s1} = 63$ and $i_{s2} = 64$, using the same ramped sinusoid. The early-time electric field distribution throughout the 1-D grid is plotted in Fig. 1 for the two types of current sources. Fig. 1(a) clearly shows the detrimental effect of the single source. The spatial grid-based oscillation illustrates the well-known Gibbs phenomenon. Fig. 1(b) shows the corresponding result for the case of twin current source.

Fig. 2 illustrates why the compact source spanning only two spatial grid cells alleviates the problem of Gibbs phenomena. Using (2)–(4), we choose the amplitude of $f(t)$ used in the twin source to give the same radiated wave amplitude as that generated by the single source. Dashed and dotted–dashed lines are used to plot the electric fields generated by simulations with a single source located at either $i_s = 63$ or $i_s = 64$. A solid line is used to plot the electric field distribution generated by the twin source. We see that this latter result passes through the

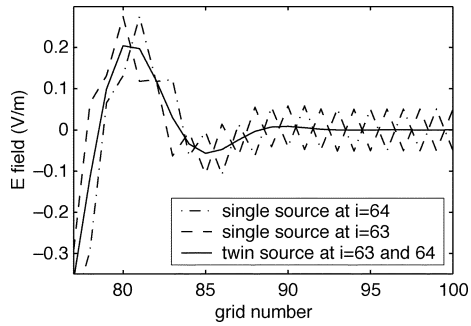

Fig. 2. Performance comparison of single- and twin-source conditions. (Only part of the grid of Fig. 1 is shown here.)

center of the set of ripples present in the electric field distributions generated by each single source. These results clearly demonstrate that the effect of linear superposition completely cancels the error in the case of the twin-source scheme.

In a hard source implementation, the field component at the location of the source is assigned the desired temporal driving function

$$E_z|_{i_s}^{n+1} = f(t)|^{n+1}. \quad (5)$$

Since the hard source implementation scatters any energy incident upon the source location, the electric field component of the wave launched by a twin source is determined by only one of the two sources. In other words, for $f(t) = A_o \sin(\omega t + \phi)$, the field observed at $x_{\rm obs} > 0$ depends only on the source located at $\Delta x/2$ as follows:

$$E_z(x_{\rm obs}, t) = A_o \sin\left[\omega t - k_x\left(x_{\rm obs} + \frac{\Delta x}{2}\right) + \phi\right] \quad (6)$$

Similarly, the field observed at $x_{\rm obs} < 0$ depends only on the source located at $-\Delta x/2$. For the same reasons discussed previously in the case of the current source, a single hard source produces errors due to the Gibbs phenomenon while a twin-source scheme eliminates the error.

III. Numerical Examples

In this section, we present the results of two numerical experiments which illustrate the successful use of the proposed compact wave source condition in a 2-D PSTD grid. For each case, the performance of the compact multisource scheme is compared with the problematic single-source scheme using graphical illustrations of the field distributions in space and the field evolution in time. We note that the computational domain in all simulations is terminated with UPML [7] to eliminate the wrap-around effect caused by the FFTs [1].

First, we model optical wave propagation in a 2-D TM_z dielectric slab waveguide. The waveguide consists of a core guiding layer $(\varepsilon_r = 4.84)$ and adjacent cladding layers $(\varepsilon_r = 4)$. The thickness of the core is chosen to be 0.682 μm. A modulated Blackman–Harris (BH) pulse covering a frequency range of 166–234 THz is used as the temporal driving function. The fundamental mode profile is excited at the left end of the waveguide using either one linear array or two adjacent linear arrays of hard sources. Each array spans the entire cross-section

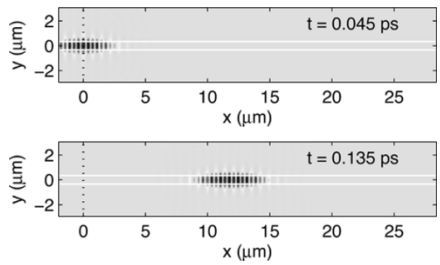

Fig. 3. Visualizations of a pulse propagating in a dielectric slab waveguide. The fundamental waveguide mode has been excited using a twin-source scheme. The white solid and black dotted lines indicate the waveguide geometry and the source location, respectively.

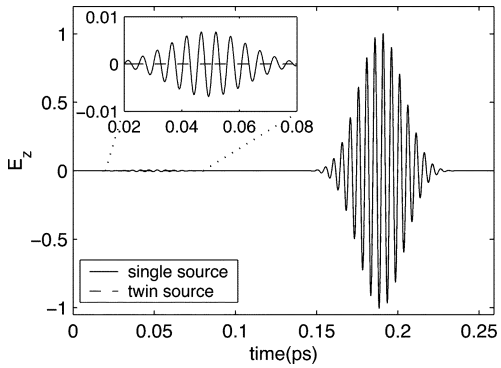

Fig. 4. Temporal evolution of the electric field at an observation point in the waveguide core for two different source conditions.

(y-axis) of the computational domain. The single linear array represents a spatial delta function along the x-direction, and is therefore problematic for the reasons outlined previously. The two adjacent linear arrays represent a twin source condition along the x-direction, thereby illustrating a practical extension of the compact 1-D source condition discussed in Section II. The hard sources are weighted along the y-axis by the transverse fundamental mode profile of the waveguide structure. The transverse array in the single source condition is located at $i = i_s$, which is treated as the origin of the x-axis, while the two adjacent arrays in the twin source condition are located at $i = i_s$ and $i = i_s - 1$. The grid resolution in the x and y directions is chosen to be approximately ten cells per smallest wavelength of interest.

Fig. 3 shows the PSTD-computed electric field distribution throughout the waveguide when the twin source condition is used. At $t = 0.045$ ps, the source is active; the pulse is being excited. At $t = 0.135$ ps, the source is no longer active because the pulse has been launched. To compare the performance of the twin- and single-source schemes, we plot the temporal evolution of the electric field observed at $x = 18.9\ \mu\text{m}$, $y = 0\ \mu\text{m}$, as shown in Fig. 4. Because it takes 0.139 ps for the pulse to propagate from the source plane to the observation plane, any energy that appears at the observation point before this time is a nonphysical artifact of the simulation. When the single-source scheme is used, a nonphysical artifact appears within this early-time window. The artifact exactly follows the time variation of the temporal driving function of the source, clearly indicating that it is caused by the problematic single-source scheme. This sort of artifact would cause significant errors in a number

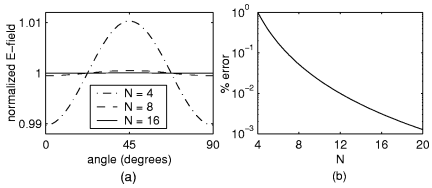

Fig. 5. Anisotropy of a wave radiated by four electric current line sources configured as a quadruplet source. (a) Analytically determined electric field amplitude is plotted at a distance of 8λ from the center of the source, as a function of the angle of observation. N corresponds to the grid sampling density, which dictates the spacing between the current sources. (b) Maximum deviation (percent error) in the field amplitude as a function of grid resolution.

of practical optical waveguide simulations wherein quantitative data such as the propagation constant is extracted from the numerical data. The twin-source scheme does not exhibit this artifact.

Second, we investigate the implementation of the compact source condition for the excitation of a cylindrical wave in a 2-D TM_z grid. In this example, the transparent current source condition is comprised of a twin source in both the x and y directions. We call this a quadruplet source since the source condition spans a total of four grid cells. Here, we consider the case of a square lattice ($\Delta x = \Delta y$) for which the quadruplet source exhibits four-fold rotational symmetry. Before presenting simulation results, we address the issue of anisotropy introduced by the quadruplet source. The analytical solution for the fields radiated by an ideal electric line source and the principle of linear superposition are used to construct the analytical solution for a quadruplet source. Fig. 5(a) shows the analytical electric field amplitude at a distance of $r = 8\lambda$ from the center of the quadruplet source, as a function of the observation angle, θ, with respect to the x-axis. The spacing between the individual line sources is chosen to represent a single grid cell in either direction; three different grid resolutions are considered: $N = 4, 8$, and 16, where $N = \lambda/\Delta x$. For each case, the field amplitude in Fig. 5(a) has been normalized by the average value across all angles, in order to permit direct comparison of the anisotropy across the three cases. As the grid resolution increases, the analytical solution for the quadruplet source converges to that of a single source which radiates isotropically. The degree of anisotropy introduced by the quadruplet source is quantified in terms of the maximum deviation in the electric field amplitude (relative to the unit-amplitude wave radiated isotropically by a single source). The maximum deviation occurs at observation points along the main grid axes (0° and 90°) and the grid diagonals (45°). Fig. 5(b) shows the maximum deviation as a percent error in the normalized field amplitude. For grid resolutions of $N \geq 6.84$, the anisotropy error is less than 0.1%. We note that the degree of anisotropy introduced by the quadruplet source does not vary significantly with observation distance.

In our 2-D test simulations, a modulated BH pulse covering a frequency range of 0.1–100 THz is used as the temporal driving function. The size of the computational domain is 128×128 cells. The grid resolution in the x and y direction is chosen to be $N = 8$ for the smallest wavelength of the wave launched from the source. The wave is excited using either a single current source located at $i_s = j_s = 32$ or four current sources (the quadruplet source) located at $i_{s1} = i_{s2} = j_{s1} = j_{s3} = 32$

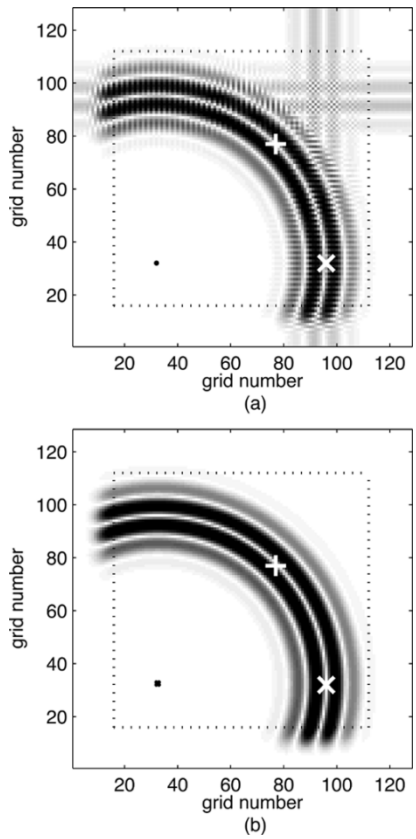

Fig. 6. Visualizations of the electric field distribution in a 2-D TM_z PSTD domain after a pulse has been launched by a compact electric current source (marked by the black dot(s) in the lower left corner of the domain). Two different source schemes are compared: (a) single source and (b) quadruplet source. The dotted-line box inside the grid boundaries marks the UPML interface. Observation points where the field is recorded as a function of time and plotted in Fig. 7 are marked by the $+$ and x symbols.

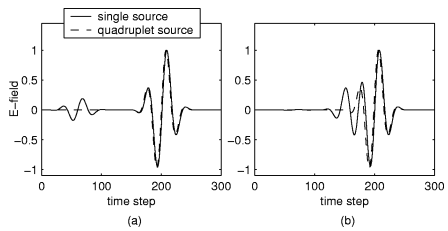

Fig. 7. Temporal evolution of the electric field at the observation points marked by the (a) $+$ and (b) x symbols in Fig. 6 for two different source conditions.

and $i_{s3} = i_{s4} = j_{s2} = j_{s4} = 33$. In Fig. 6, we compare the PSTD-computed electric field distributions for these two test cases. Fig. 6(a) shows that the wave launched by the single source scheme exhibits erroneous disturbances in the field pattern. This error is present in the PSTD domain even when the source is no longer active (as is the case at time step 200). Fig. 6(b) shows that the quadruplet source scheme successfully launches a cylindrical wave without any of the previously observed artifacts.

To further compare the performance of the single- and quadruplet-source schemes, we plot the temporal evolution of the electric field observed at two different locations in the grid representing observation angles of $\theta = 0$ and $\theta = 45°$. Fig. 7(a) shows the field observed at ($i_1 = 96$, $j_1 = 32$), marked by the x in Fig. 6. This temporal waveform exhibits phenomena that is qualitatively similar to that observed in the waveguide case; that is, a nonphysical artifact appears in the early-time window when the single-source excitation is used. However, we note that the magnitude of the artifact produced by the single source here is much larger than observed in the waveguide. This increased error can be attributed to the fact that the source in this experiment is compact in both dimensions, whereas the source in the waveguide experiment was compact in only one dimension. Fig. 7(b) shows the field observed at ($i_1 = 77$, $j_2 = 77$), marked by the $+$ in Fig. 6. The artifact induced by the single source is very small in an early-time window. However, the pulse is severely distorted. In the case of the quadruplet-source scheme, neither the early-time disturbance nor the pulse distortion is observed.

IV. Conclusion

In this letter, we have addressed the issue of source implementation in the PSTD algorithm. Using 1-D PSTD simulations, we have shown that a compact source spanning only two spatial grid cells completely eliminates the problem of Gibbs phenomena. Numerical investigations have revealed that the error introduced by one of the two adjacent sources exactly cancels the error introduced by the other. In 2-D PSTD simulations, we extended the compact "twin-source" scheme to demonstrate error-free excitation of waveguide modes and cylindrical waves.

References

[1] Q. H. Liu, "The PSTD algorithm: a time-domain method requiring only two cells per wavelength," *Microwave Opt. Technol. Lett.*, vol. 15, pp. 158–165, June 1997.

[2] A. Taflove and S. Hagness, *Computational Electrodynamics: The Finite-Difference Time-Domain Method*, 2nd ed. Boston, MA: Artech House, 2000.

[3] Q. H. Liu, "Large-scale simulations of electromagnetic and acoustic measurements using the pseudo-spectral time-domain (PSTD) algorithm," *IEEE Trans. Geosci. Remote Sensing*, vol. 37, pp. 917–926, Mar. 1999.

[4] Q. H. Liu and G. X. Fan, "Simulations of GPR in dispersive media using a frequency-dependent PSTD algorithm," *IEEE Trans. Geosci. Remote Sensing*, vol. 37, pp. 2317–2324, Sept. 1999.

[5] T. W. Lee and S. C. Hagness, "Pseudo-spectral time-domain methods for modeling optical wave propagation in second-order nonlinear materials," *J. Opt. Soc. Amer. B*, vol. 21, no. 2, pp. 330–342, Feb. 2004.

[6] Q. Li and Y. Chen, "Pseudo-spectral time-domain analysis using an initial condition excitation technique for elimination of Gibbs phenomena," *Chinese J. Electron.*, vol. 9, pp. 92–95, Jan. 2000.

[7] S. D. Gedney, "An anisotropic perfectly matched layer-absorbing medium for the truncation of FDTD lattices," *IEEE Trans. Antennas Propagat.*, vol. 44, pp. 1630–1639, Dec. 1996.